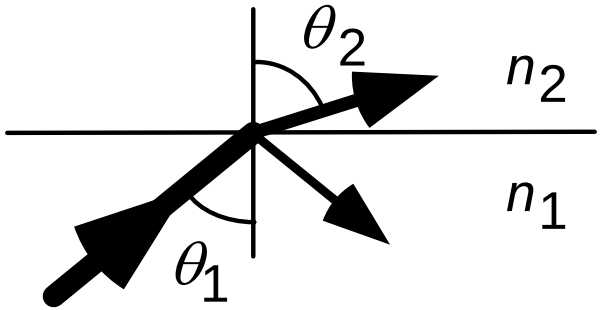

Figure 27.1 Refraction of light at the interface between two optical materials of different refractive indices.

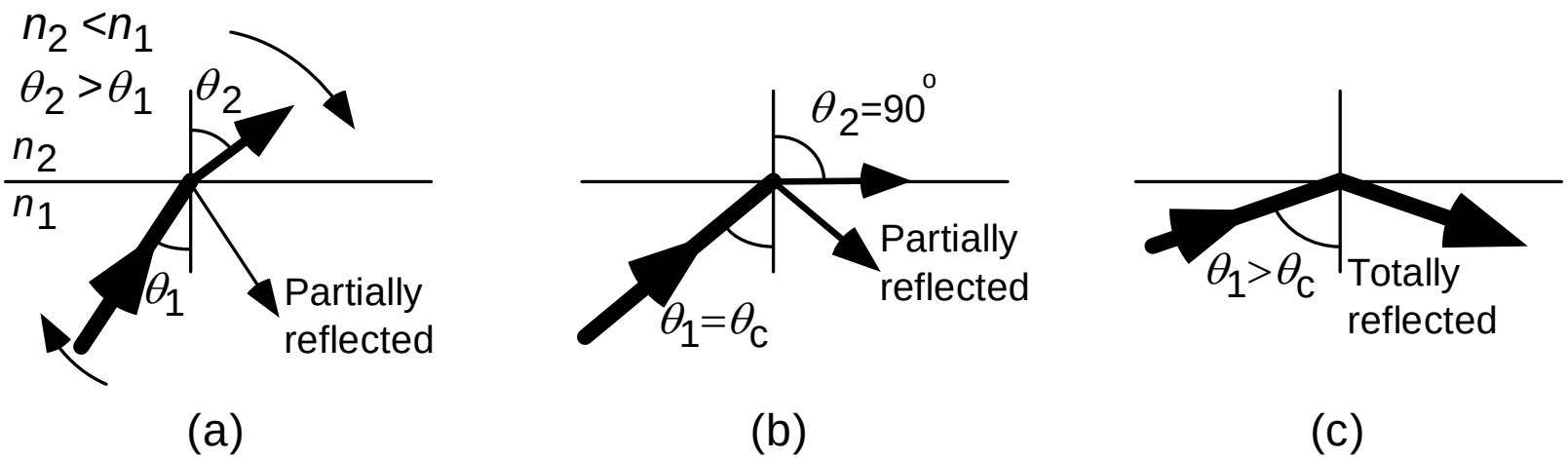

Figure 27.2 (a) and (b): Refraction and partial reflection when the angle of incidence is less than and equal to the critical angle, respectively. (c): Total internal reflection occurs when the angle of incidence is greater than the critical angle.

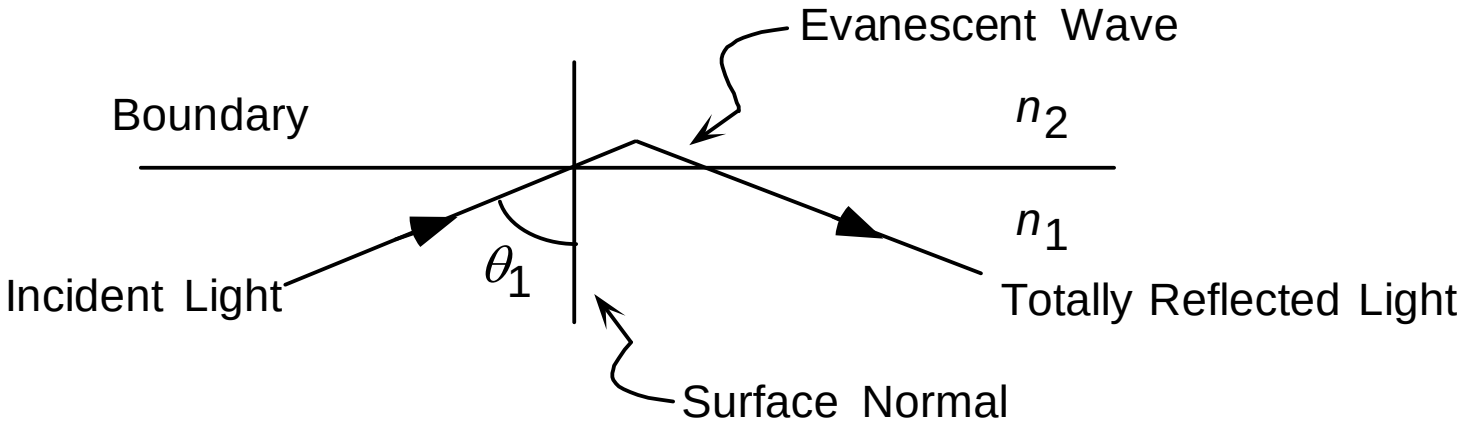

Figure 27.3 Evanescent wave penetrates into the low index side of the boundary during total internal reflection. $n_1 > n_2$ and $\theta_1 > \theta_c$.

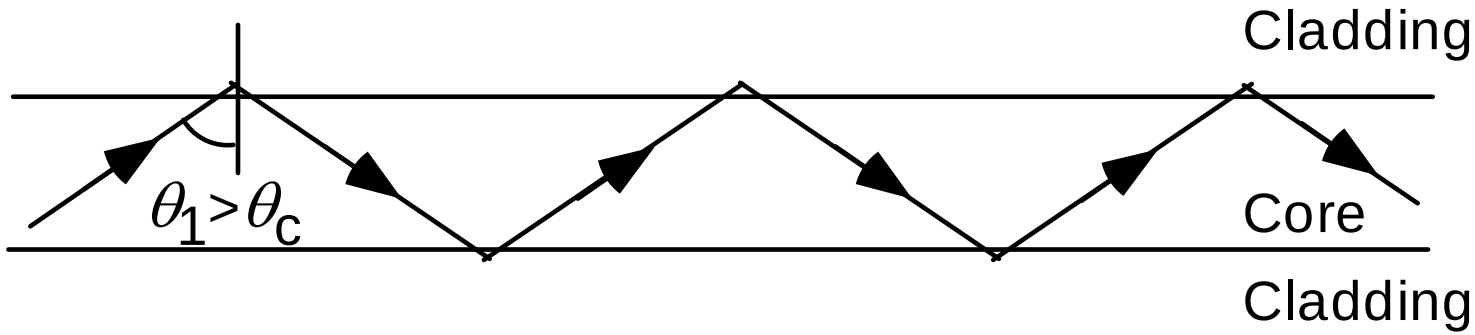

Figure 27.4 Planar optical waveguide, a high index core is sandwiched between two cladding layers of lower index materials.

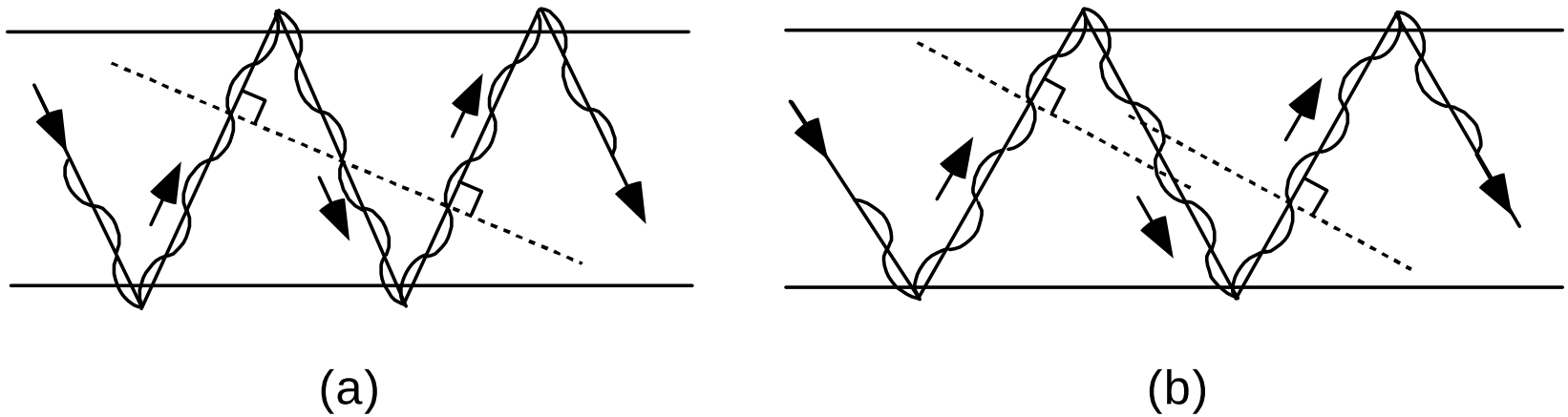

Figure 27.5 The reflected light is in phase (a) and out of phase (b).

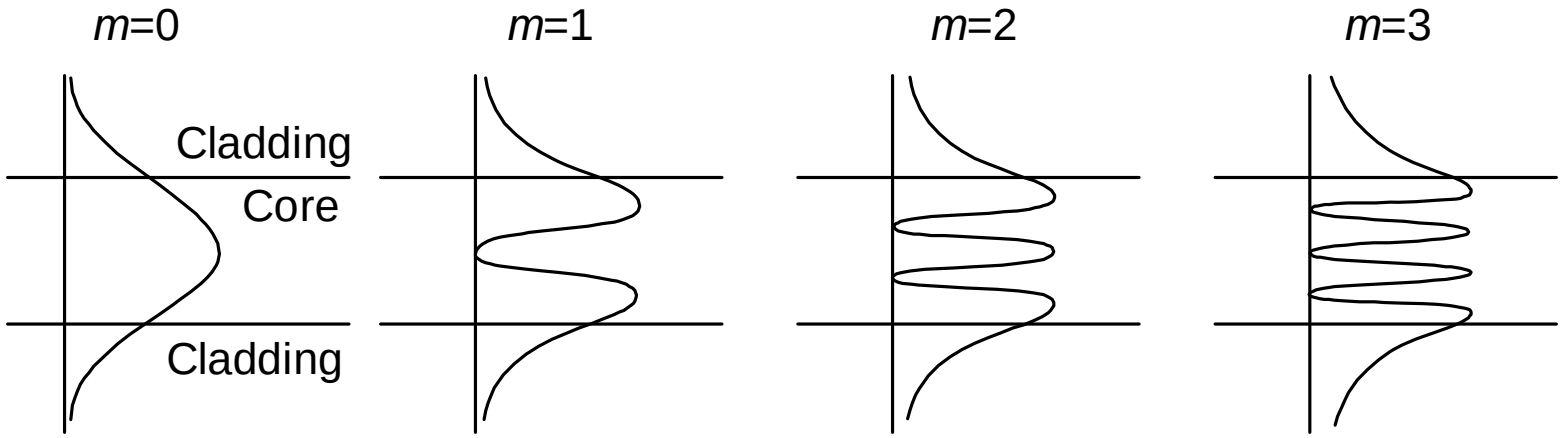

Figure 27.6 The intensity patterns of the 0th through 3rd mode of a planar waveguide.

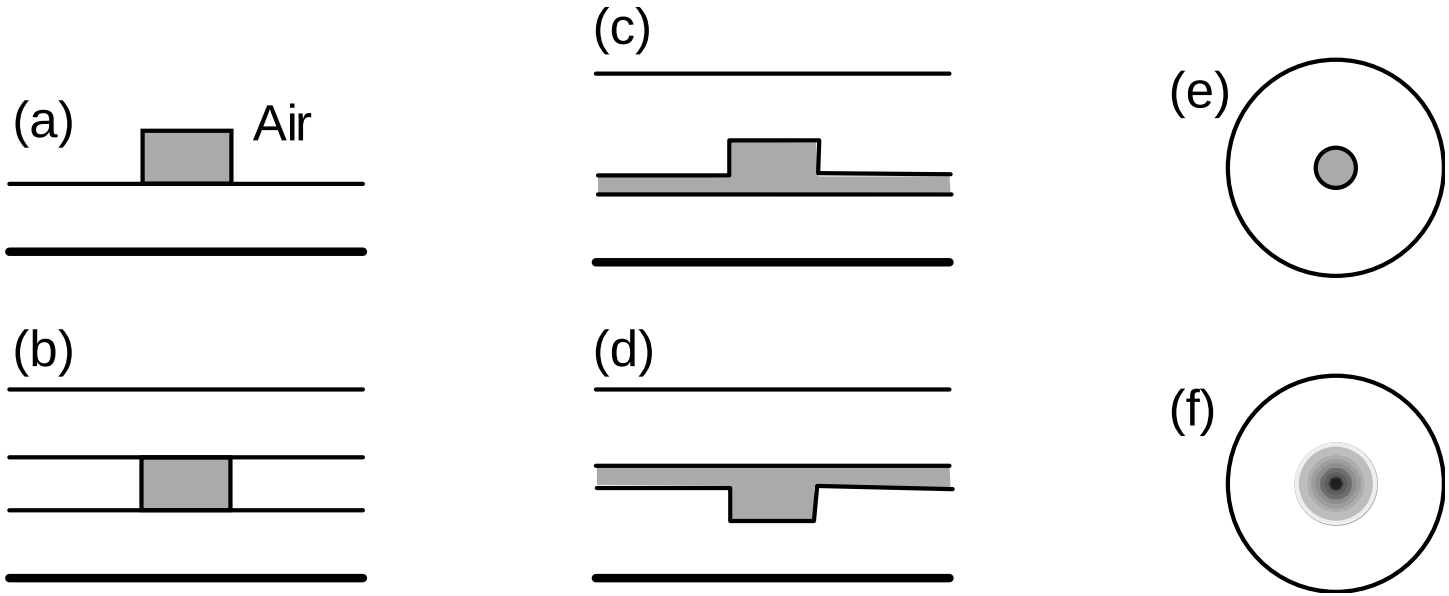

Figure 27.7 Cross-sections of several channel waveguides. (a) Air cladded channel. (b) Buried channel. The cladding around the core can have different indices. (c) Ridge or rib waveguide. (d) Inverted ridge. (e) Step index fiber. (f) Graded-index fiber, in which the index of the core gradually decreases from the center of the fiber.

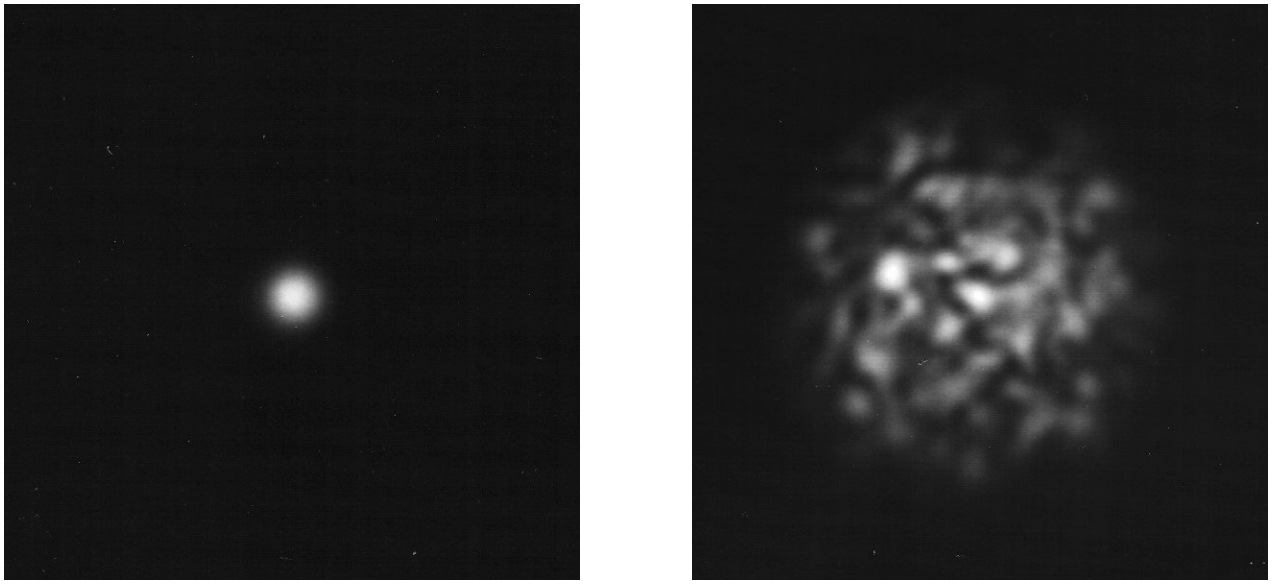

(a) (b)

Figure 27.8 Optical power distributions of (a) a single mode and (b) a multimode fiber. The two pictures have the same scale. Both fibers are made of silica glass. The diameter of the core is 9 mm for the single mode fiber, and 62.5 mm for the multimode fiber.

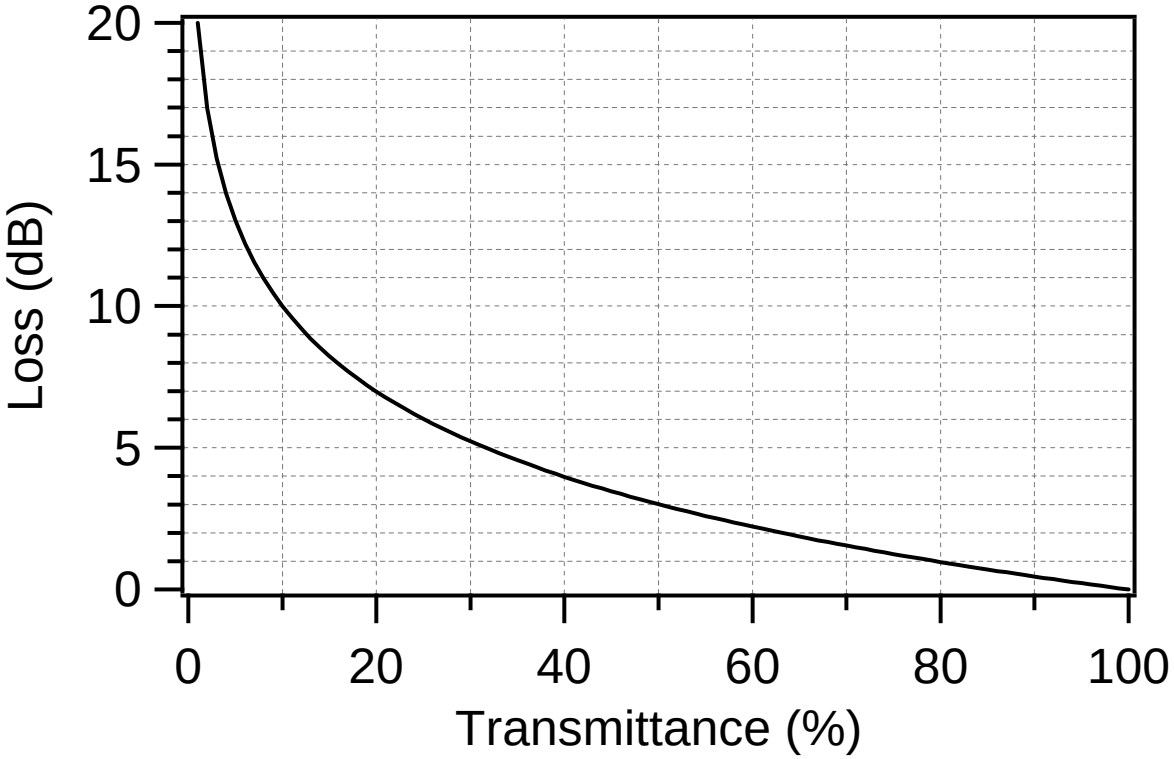

Figure 27.9 Conversion between percentage of transmitted light and loss in dB.

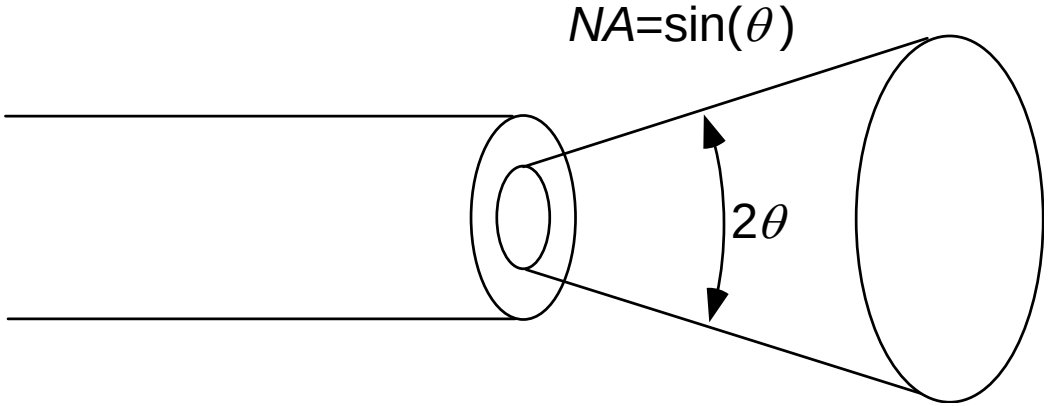

Figure 27.10 The numerical aperture of optical fiber.

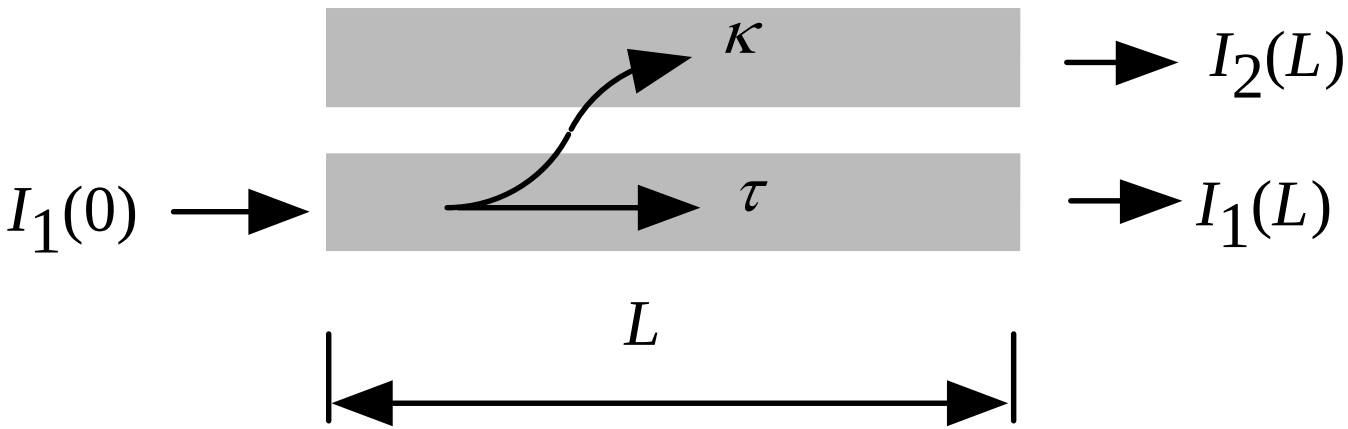

Figure 27.11 The coupling of light between waveguides. κ and τ are coupling coefficients. κ is the percentage of the initial electric field that is coupled into a second waveguide, and τ is the percentage of the electric field remaining in the original waveguide. Because optical power is proportional to the square of the electric field and total optical power is conserved, $\kappa^2 + \tau^2 = 1$.

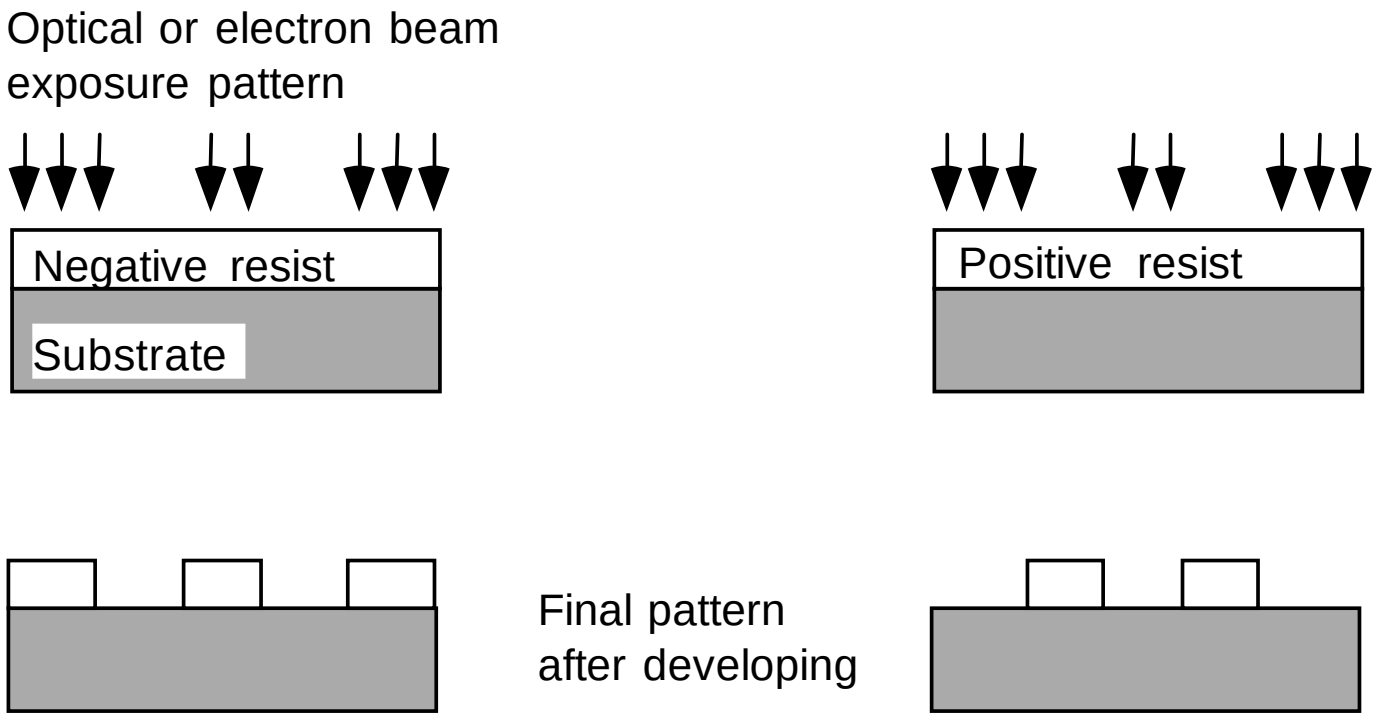

Figure 27.12 Patterning negative and positive photo- or e-beam polymers.

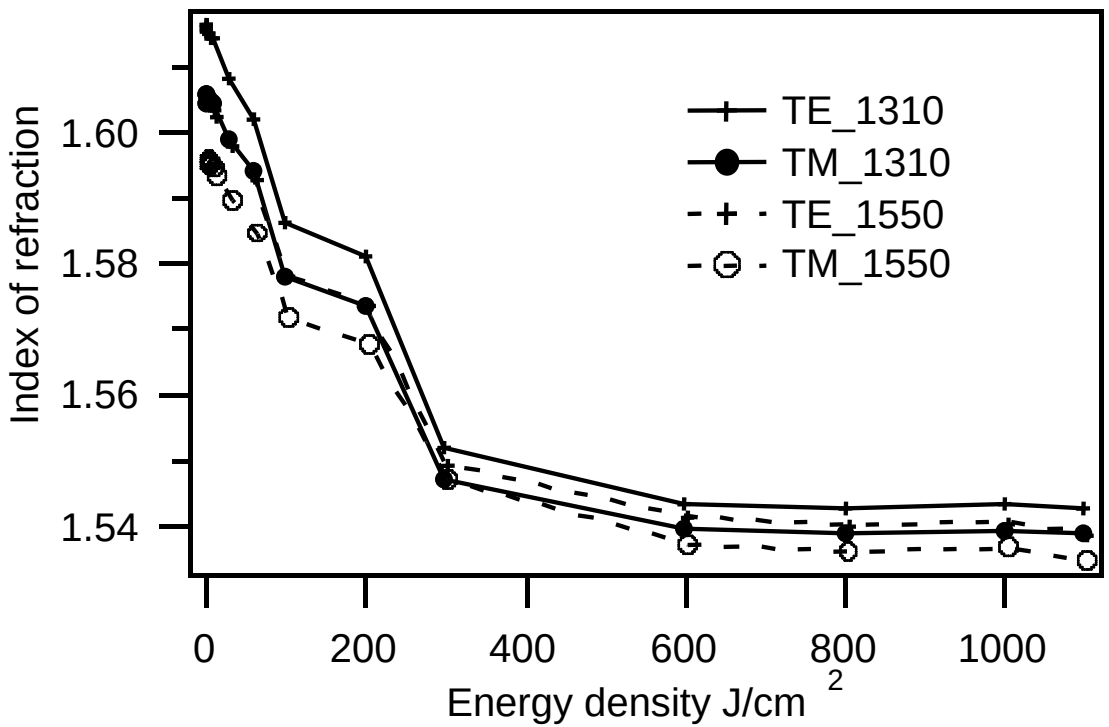

Figure 27.13 The change of refractive index of polymer AJL8/APC thin film as a function of photobleaching energy density. The peak wavelength of the UV lamp is 365 nm.

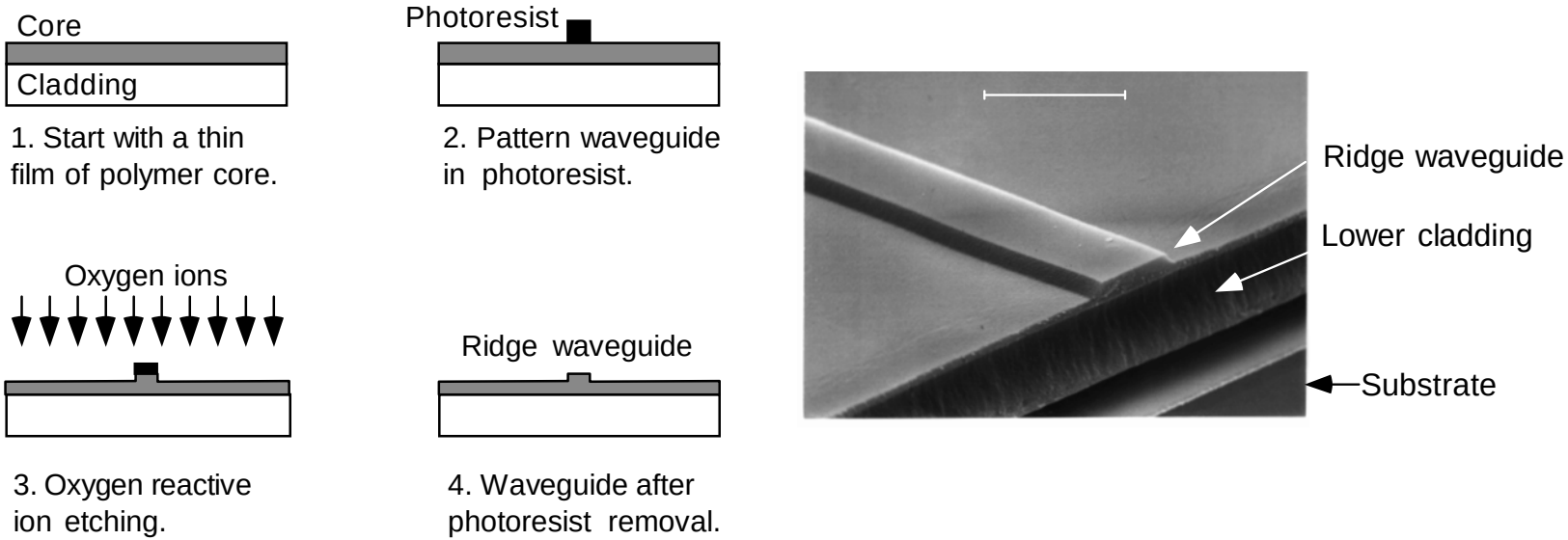

Figure 27.14 A schematic process of photolithography and RIE, and a scanning electron microscopy (SEM) image of a ridge waveguide made with this method. The scale bar at the top of the SEM image is 5 μm.

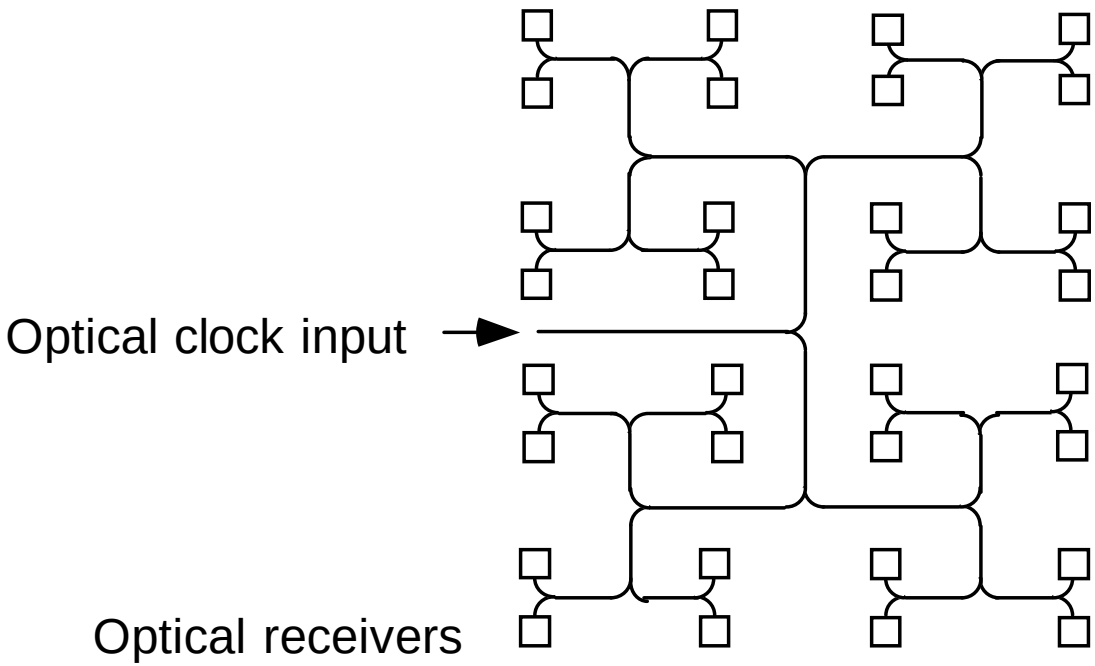

Figure 27.15 H-tree waveguide structure for synchronized clock distribution. Each branch splits the optical power equally. The waveguides between the clock input and each receiver have the same length.

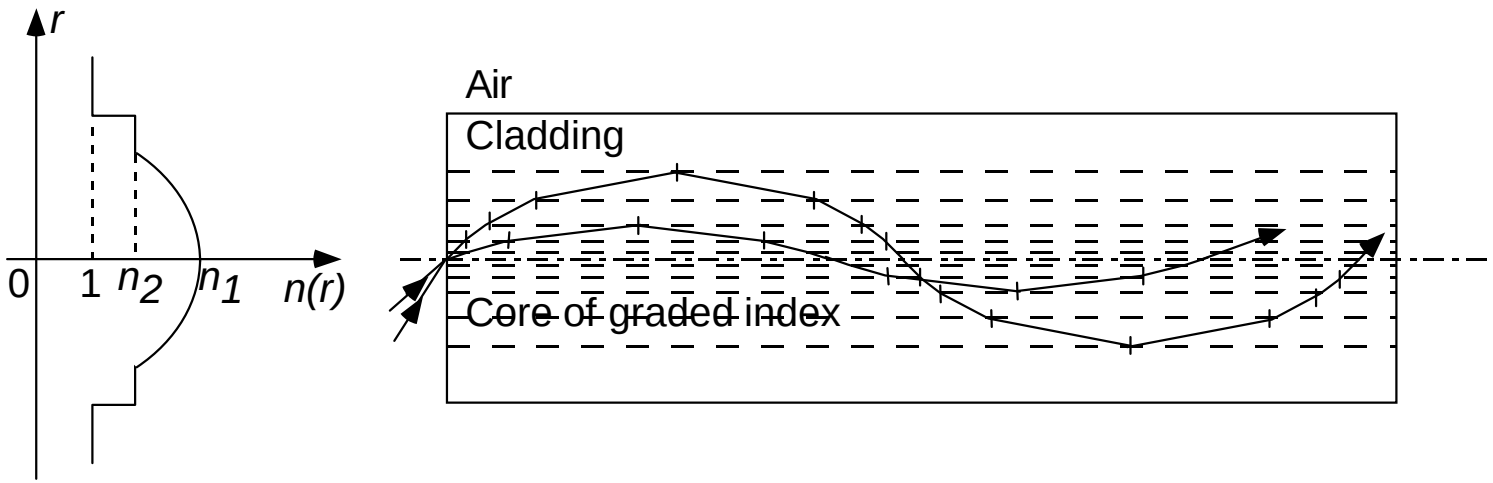

Figure 27.16 Bending and total internal reflection of light in a graded index fiber. *r* is the radius of the fiber.

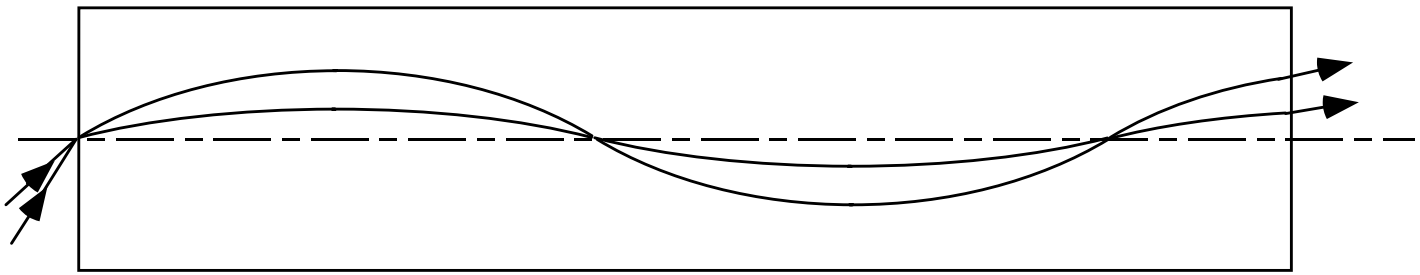

Figure 27.17 Different sinusoidal paths of light have the same period in a graded index fiber with parabolic index profile. Light ray at a larger angle has a longer path, but most of the path is in the low index zones where light travels faster. In the end, light of different paths take the same time to travel between foci.

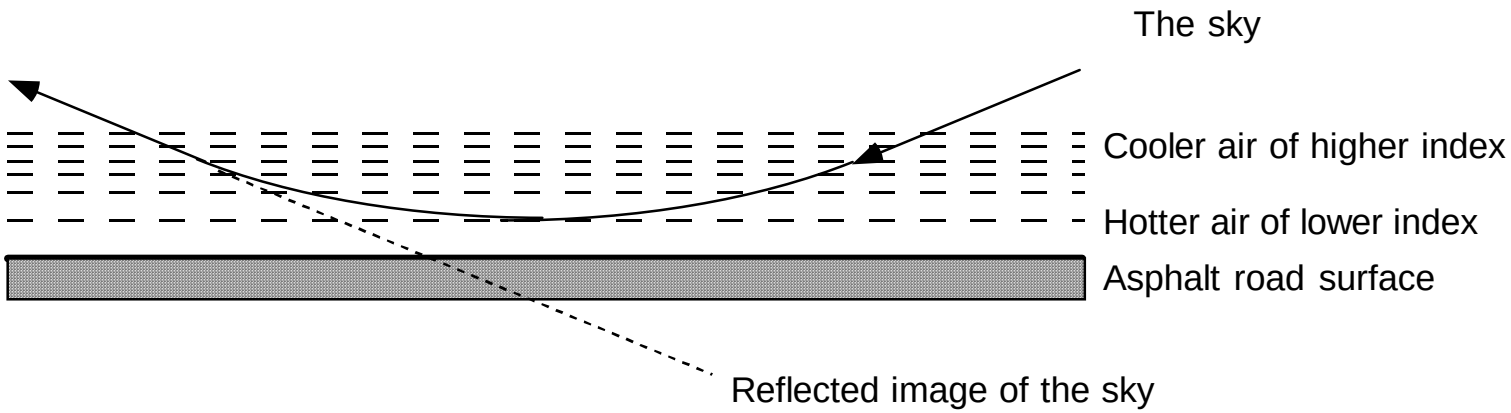

Figure 27.18 Highway mirage due to the graded index of air near the hot surface of the road.

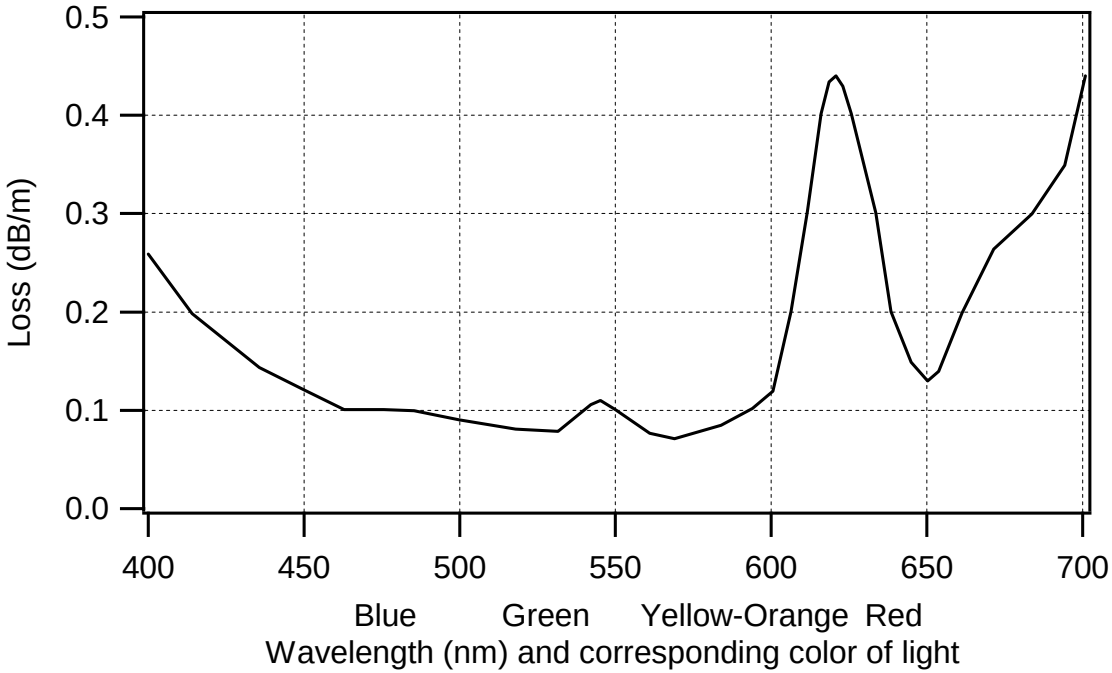

Figure 27.19 The loss spectrum of typical PMMA fiber.

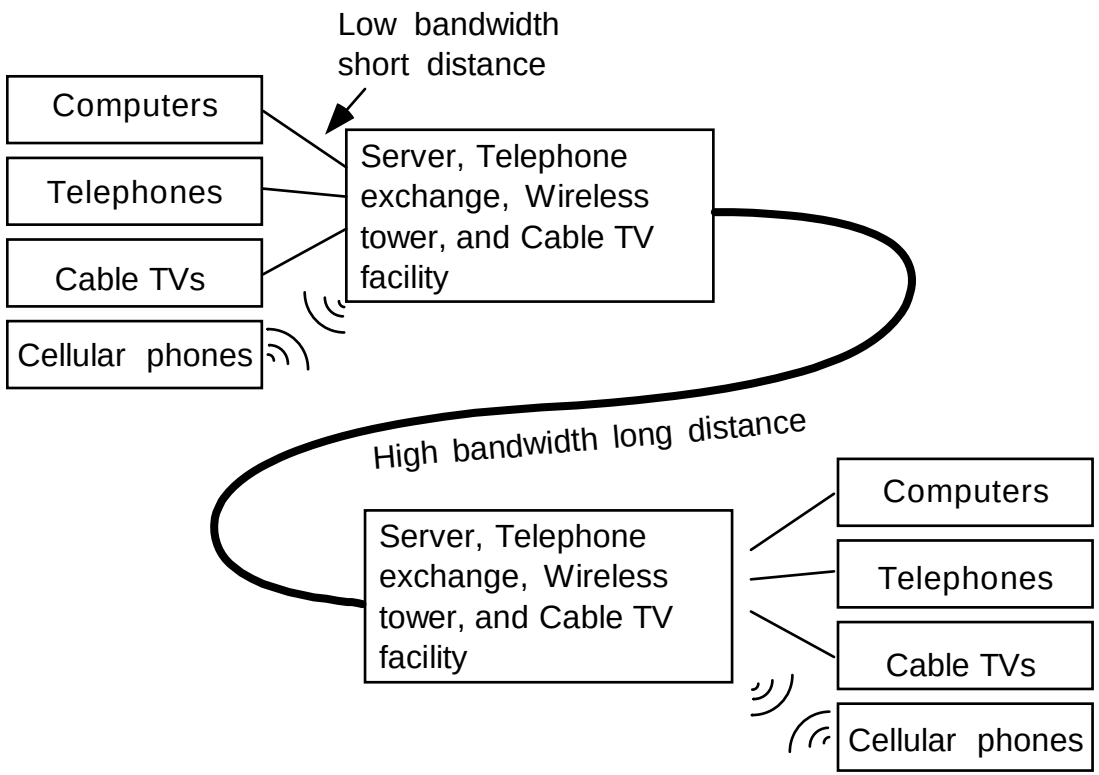

Figure 27.20 A schematic diagram of telecommunication. Low bandwidth signals between user equipment and fiber optic terminal equipment are typically transmitted through electrical cables or wireless channels over a short distance. Signals from multiple users are combined into high bandwidth optical data and transmitted through optical fiber over long distance.

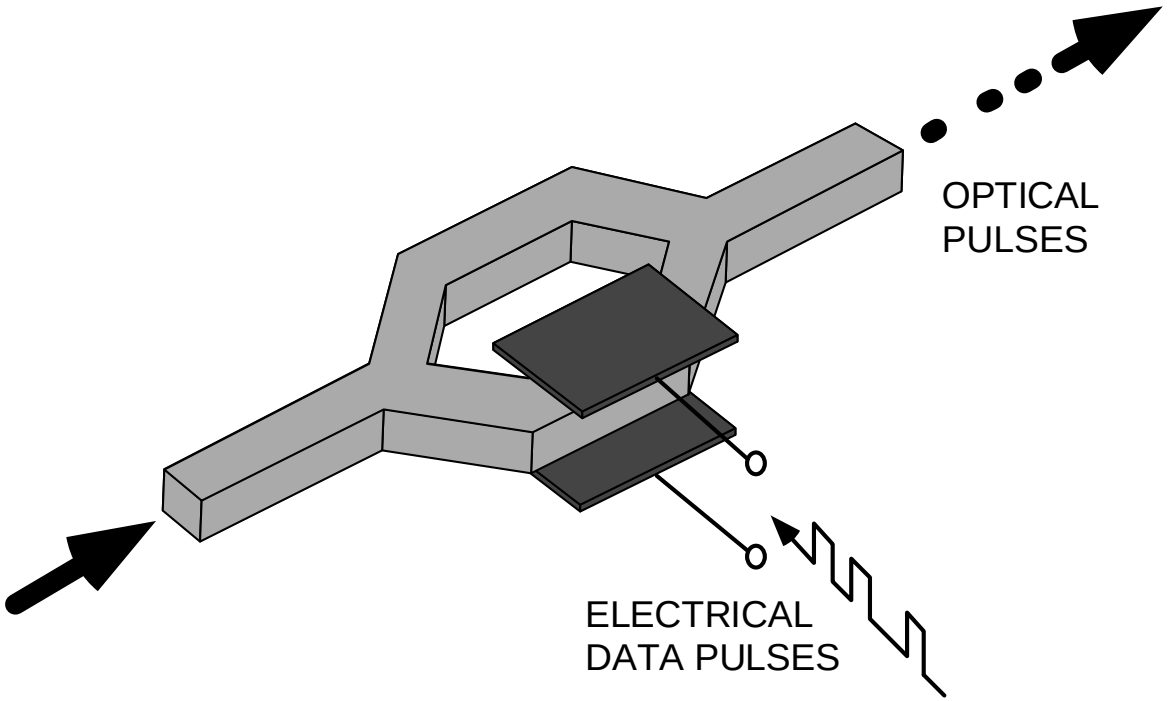

Figure 27.21 Mach-Zehnder modulator.

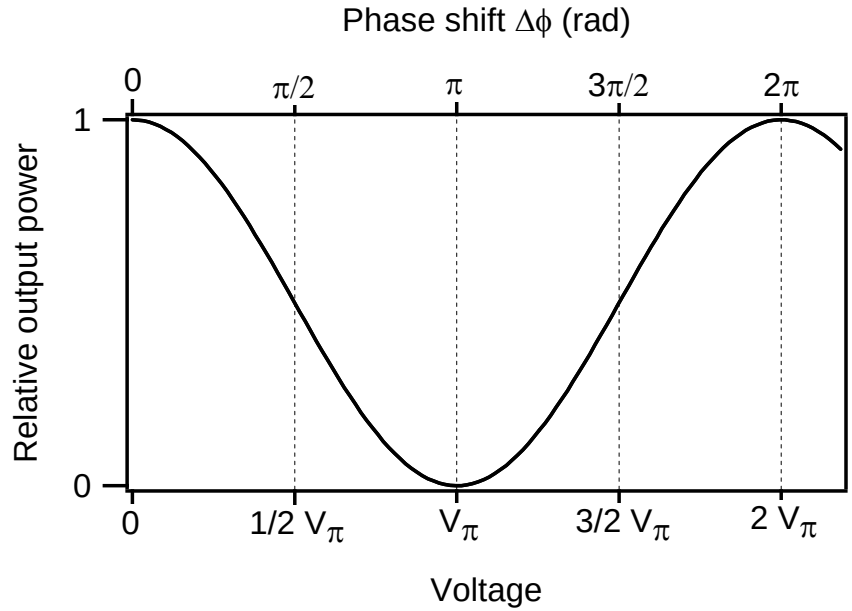

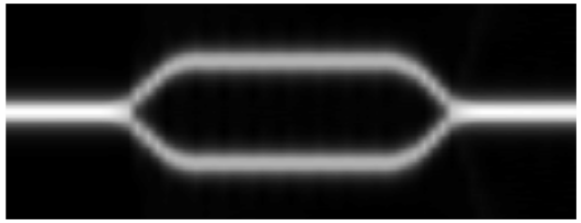

$V = 0$ and $V = 2V_\pi$

100% transmission

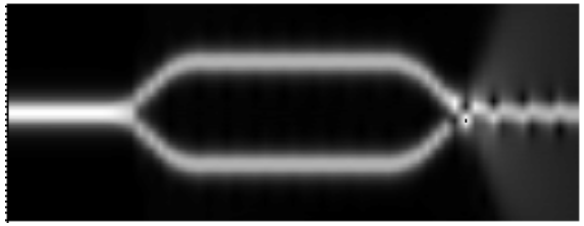

$V = \frac{1}{2}V_\pi$ and $V = \frac{3}{2}V_\pi$

50% transmission

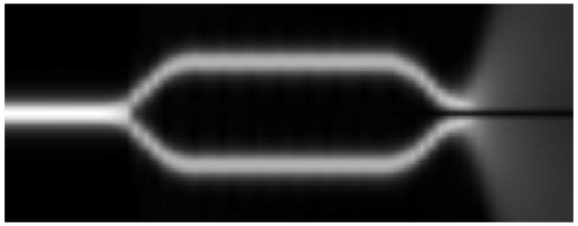

$V = V_\pi$

0% transmission

Figure 27.22 Top: Dependence of modulator output on the phase difference and applied voltage. Bottom: Optical power distribution in the modulator at various voltages.

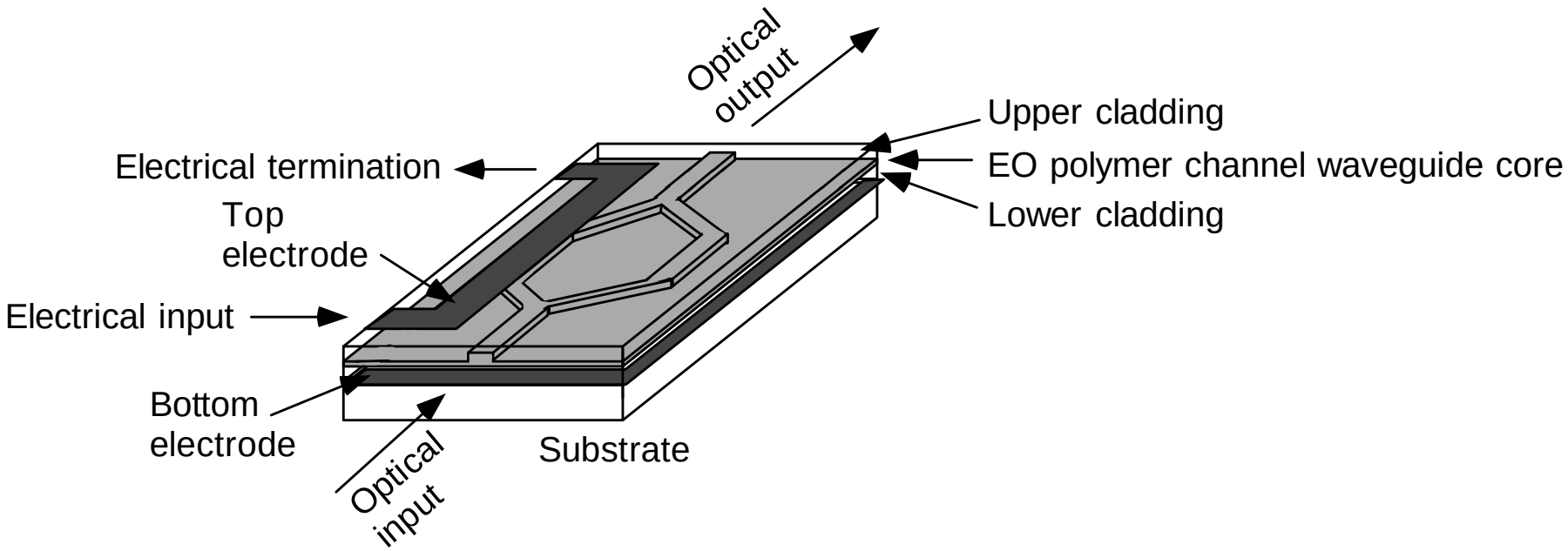

Figure 27.23 The structure of a typical EO polymer modulator.

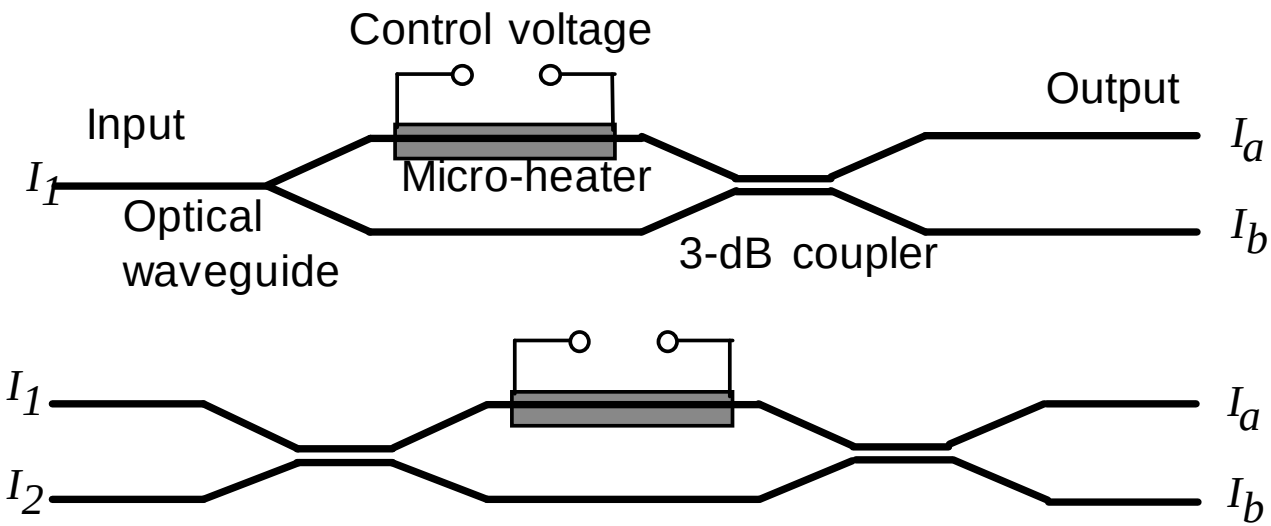

Figure 27.24 1×2 and 2×2 thermo-optic switches based on Mach-Zehnder interferometers.

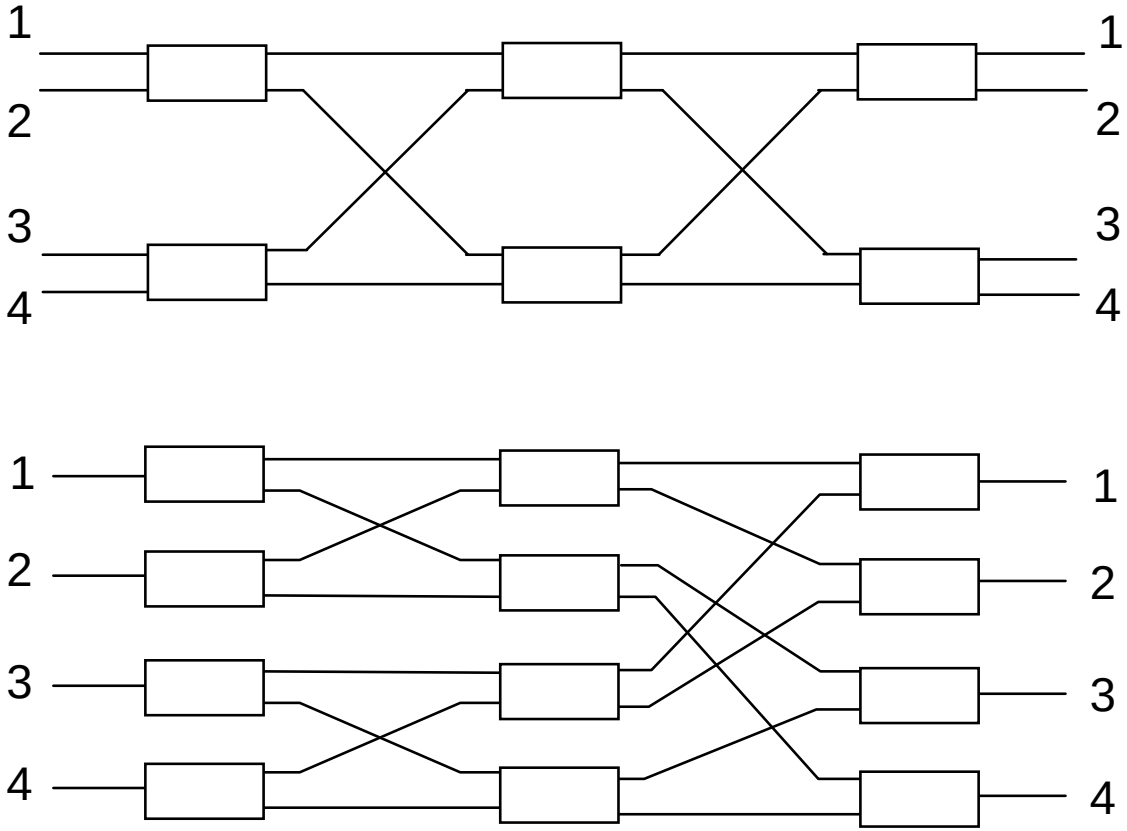

Figure 27.25 4×4 switches made of 2×2 (top), and a combination of 1×2 and 2×2 (bottom) switch elements.

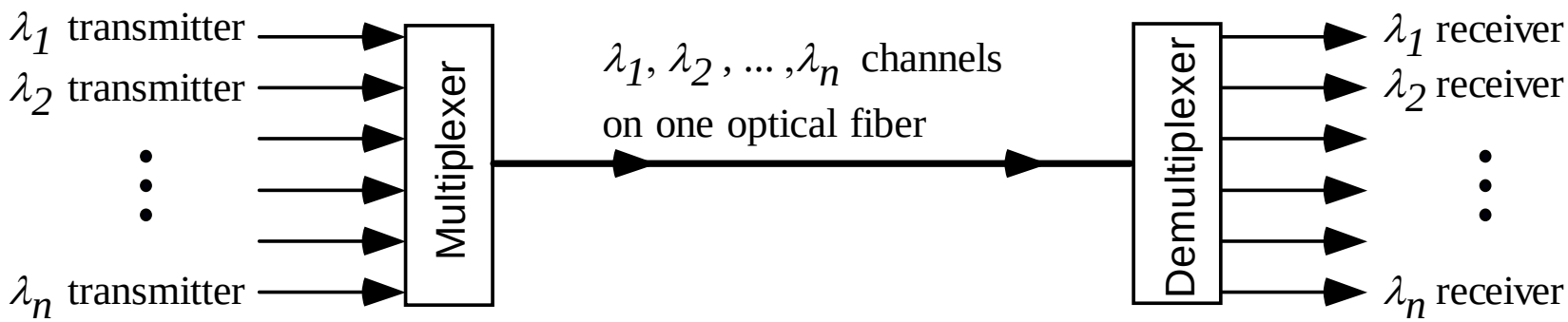

Figure 27.26 WDM transmission between two communication points.

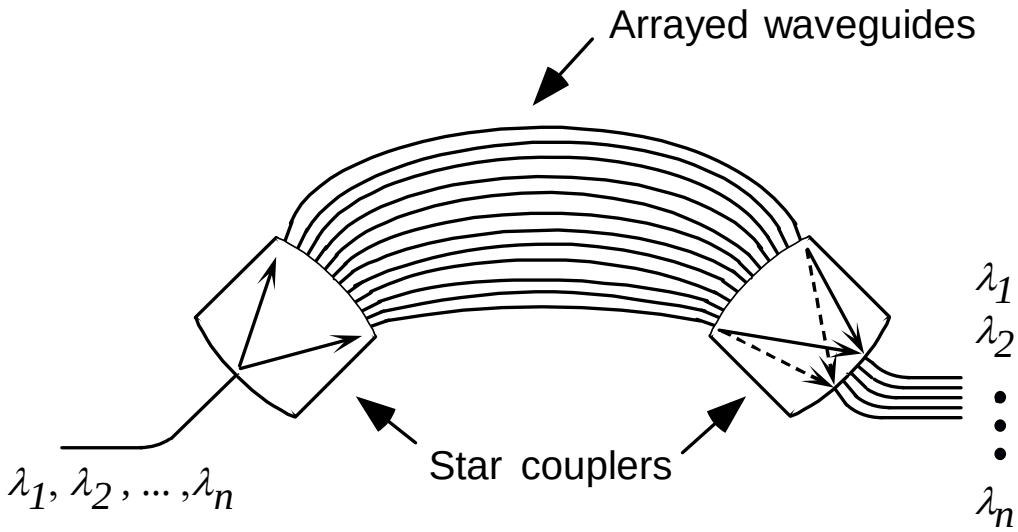

Figure 27 Arrayed waveguide grating wavelength filter. The number of waveguides in the array is typically about 100.

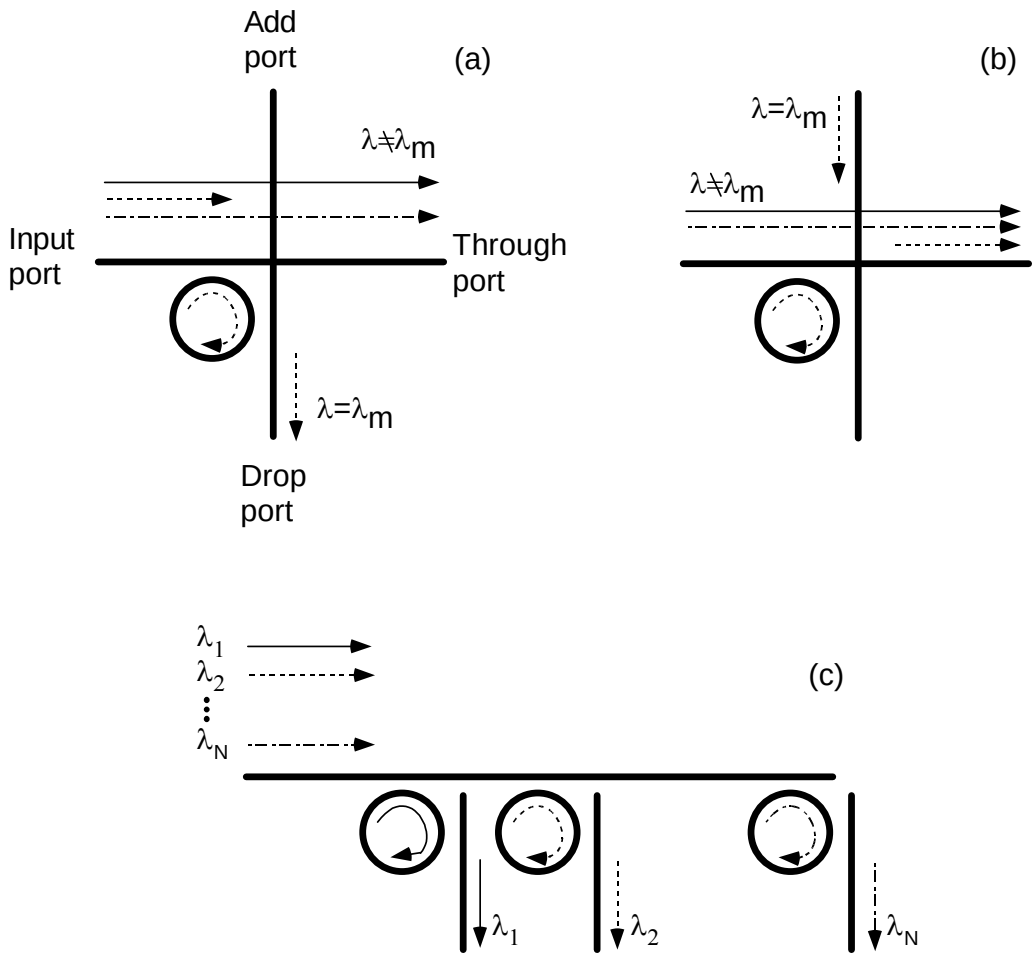

Figure 27.28 Wavelength add-drop filters based on micro-ring resonators. (a) Dropping a wavelength channel. (b) Adding a wavelength channel. (c) WDM filter demultiplexer made with micro-ring resonators.